



Influence of chlorite treatment on the fine structure of alkali pretreated sugarcane bagasse

Subhajit Kundu¹ · Debarati Mitra¹ · Mahuya Das²

Received: 11 August 2020 / Revised: 7 October 2020 / Accepted: 29 October 2020 / Published online: 7 January 2021
© Springer-Verlag GmbH Germany, part of Springer Nature 2021

Abstract

Bagasse, an industrial agro waste is treated with alkali initially to remove hemicelluloses fraction followed by treatment with sodium chlorite solution varying the treatment time. The novelty of the work lies in the bleaching with chlorite treatment in alkaline medium. The treated bagasse fiber was characterized by Fourier transform infrared spectroscopy (FTIR), X-ray diffraction (XRD), particle size analysis by dynamic light scattering technique (DLS), optical microscope, scanning electron microscope (SEM), atomic force microscope (AFM), UV spectroscope, and thermogravimetric analysis (TGA). It was found that during alkali treatment, a lattice transformation from cellulose I to cellulose II took place. Chlorite treatment removed lignin initially, and then with increasing time, the amorphous portion of cellulose is removed, rendering high crystallinity in the fiber. All the changes have been accounted by evaluation of LOI (lateral order of index), TCI (total crystallinity index), and HBI (hydrogen bond intensity) from FTIR study. XRD study also revealed the same fact. AFM study also supported the same fact indicating generation of sharp crystal and rough surface. Morphological study of treated and untreated bagasse fiber also exhibited fibrillation of fiber. Radius of hydration as estimated by DLS analysis followed a decreasing trend with increase in chlorite treatment time. The loss of transparency in cellulose fiber has been exposed by UV spectra analysis. TGA study showed that thermal stability has been increased with chlorite treatment. Such alkali treatment along with sodium chlorite for cellulose extraction from bagasse has not been performed by earlier investigators. Extracted cellulose fiber will be a very suitable reinforcing agent due to highly fibrillated morphology.

Keywords Bagasse · Cellulose · Noncellulosic material · Fibrillation · Crystallinity

1 Introduction

Cellulose, a common natural fiber, having tremendous biodegradation properties, is suitable for many potential applications. Cellulose is one of the important constituents [40] of wood, plants, some bacteria, and algae [59]. Natural fibers are lignocellulose materials which mainly comprises cellulose,

hemicellulose, and lignin. Modern world is in constant thrives to search more and more potential natural plant materials [2, 13, 29, 31, 36, 37, 48, 58, 62, 63]. Cellulose is highly abundant in plants; still the agro waste (rice straw, soybean pods, corncob, etc.) and industrial agro waste (bagasse, tomato peel, etc.) should be explored more [52]. Among this industrial agro waste, huge amount of bagasse is generated. Typically, from processing 100 t of sugarcane produces 23 t of bagasse [67]. The cellulose, hemicellulose, and lignin contents of dry bagasse were reported as $35.0 \pm 0.4\%$, $30.3 \pm 0.5\%$, and $17.0 \pm 0.7\%$, respectively, by Pathak et al. [47]. The cellulose fiber in plants is a tied combination of cellulose microfibrils which consists of the smallest cellulose fibril unit. Different techniques are available to extract the cellulose part from bagasse. Easy extraction of cellulose in the most economic way involves chemical, physical, or biological pretreatment methods to remove the hemicellulose, lignin, and other components rather than cellulose [10, 28, 30, 50]. Alkali pretreatment has been used by Sun and Cheng [61] for breaking down the

✉ Mahuya Das
d_mahuya@yahoo.com

Subhajit Kundu
subhajitkundu1992@gmail.com

Debarati Mitra
debarati.che@gmail.com

¹ Department of Chemical Technology, University of Calcutta, Kolkata 700009, India

² Greater Kolkata College of Engineering and Management, South 24 Pgs, Baruiapur, West Bengal, India

lignin structure and hence improving the susceptibility of the hemicellulose and cellulose fraction. The disruption of lignin, hemicellulose, and cellulose has been carried out with chemical treatment and physical force by Brinchi et al. [8]. Effect of alkali treatment on many plant fibers has been well investigated. Authors have reported that this treatment removes hemicellulose from the plant fiber rendering high crystallinity in the cellulose structure depending on the treatment condition. Mzimela et al. [44] have investigated the effect of alkali treatment on sugarcane bagasse and reported about increase in aspect ratio and crystallinity with dissolution of matrix material. Sodium chlorite has been used to remove lignin from the plant fiber and to extract cellulose effectively, but works on plant fiber with chlorite treatment variation have not been studied too much. Chlorite treatment brings out delignification of natural fiber and affects other polysaccharide rendering suitable property modification of cellulose fiber [68]. Kumar et al. [34] reported the adverse effect of acid chlorite delignification on cellulose chain length. Mohomane et al. [41] have also studied the kinetics of thermal degradation of alkali-treated delignified sugarcane bagasse and also reported improve in crystallinity of bagasse fiber by treatment. Lazic et al. [38] studied the effect of alkali treatment and chlorite treatment on flax fiber thoroughly to extract cellulose fiber which is much whiter and acquires higher surface area, higher wetting ability hence better suitability to composite fabrication. Another observation has been reported by Lazic et al. that with proper treatment conditions, chlorite treatment only leads to oxidation of the reducing end groups (aldehyde) of cellulose macromolecules to carboxylic groups, keeping higher degree of polymerization of cellulose chain, thereby increasing the aspect ratio. Mostly all these bleaching by sodium chlorite has been carried out under acidic pH. Delignification under alkali condition has also been reported using hydrogen peroxide but not with chlorite [39]. Other agents like hypochlorite, bleaching powder are also there for delignification. But among all, sodium chlorite is the most common one. Hypochlorite bleaching forms oxy cellulose resulting fibers which develops brownish stains on storage and uneven dyeing. On the other hand, chlorite bleaching does not produce oxycellulose. It is safe to fiber giving permanent whiteness without loss of tensile strength. Chlorite is not sensitive to traces of metallic contaminants, whereas peroxide shows disastrous reaction with the presence of both iron and copper. The bleaching strength of sodium chlorite is always optimum under acidic pH, and this leads to a problem of corrosion with metal container used for bleaching. Another problem associated with acid chlorite bleaching is liberation of harmful chlorine dioxide (ClO_2) gas which is negligible under alkaline condition. The study of chlorite bleaching reaction under alkaline medium is very rare [24]. It has been reported by Higginbotham and Leigh [24] that bleaching of desized cotton applying steaming by 2% sodium chlorite

solution along with 5% sodium carbonate maintaining pH at 11 is very effective reducing the pH suddenly at pH around 5. The desizing was done by 3% alkali treatment. They predicted about the observation of considerable high rate of bleaching at pH 7 and pH 8–5 that there must be certain mechanism without direct involvement of chlorine dioxide and chlorous acid.

The aim of this work is to treat bagasse by alkali first then by prolonged chlorite treatment under alkaline pH and to study the change in fine structure of bagasse cellulose by the treatment. The novelty of the work lies in the chlorite treatment of bagasse to remove lignin totally under alkaline pH. The performance of sodium chlorite in the absence of acidic medium as a fine structure modifier of bagasse is to be judged by this work. The fine structure of the fiber is an important controlling factor for composite fabrication, and the outcome of the work could develop cellulose fiber with higher aspect ratio and surface area, i.e., leading to a better wetting of fiber by polymer matrix during biocomposite fabrication.

2 Experimental

2.1 Materials

The raw material, sugarcane bagasse, was bought from local market located at Rajabazar, Kolkata. The other materials used in the process are sodium hydroxide (NaOH , >97% HPLC grade), sulfuric acid (H_2SO_4 , 98% HPLC grade), and sodium chlorite (NaClO_2 , 80% HPLC grade). All these materials were purchased from Merck, Mumbai, and were used without further purification.

2.2 Method

2.2.1 Extraction of cellulose

Sugarcane bagasse collected from local market was cut into small pieces followed by drying at 110 °C. It was then grinded into fine irreducible forms and further dried at 105 °C to remove the excess water entrapped in the material. After that it was soaked in 18% (*w/v*) NaOH solution for 1 h and then washed with tap water. It was then treated with 2% H_2SO_4 solution for 30 min and again washed with distilled water maintaining a constant pH of 7 and dried to remove the hemicellulose fraction. For the delignification step, the dried sample was treated with 2% (*w/v*) NaClO_2 solution for 1 h with constant stirring by a magnetic stirrer at constant temperature of 65 °C and then allowed to cool to room temperature. It was washed rapidly with distilled water, and the pH was maintained at 7. Then the sample was centrifuged at 5000 rpm for 15 min and then lyophilized. The sample was weighed and labeled as C1. The delignification step was repeated by varying the delignification time from 1 to 4 h with an

increment of 30 min maintaining the other conditions constant, and the samples were labeled as C1.5, C2, C2.5, C3, C3.5, and C4 respectively (Table 1).

2.3 Characterization

2.3.1 FTIR study

FTIR is a useful technique to identify the functional groups present in a sample. The cellulose samples were mixed with potassium bromide (KBr) and pressed to form a pellet which was then investigated using PerkinElmer FTIR instrument, model no. spectrum 100. The FTIR spectra were recorded in the range of 4000–450 cm^{-1} . The total crystalline index (TCI) was performed by the absorbance ratio of the peak at 1372 cm^{-1} and the strong peak at 2900 cm^{-1} . The lateral order index (LOI) and the hydrogen bond intensity (HBI) were also calculated by the ratio of absorbance at 1424 cm^{-1} /893 cm^{-1} and 3350 cm^{-1} /318 cm^{-1} , respectively [34].

2.3.2 XRD analysis

XRD determines the structure of the sample in terms of amorphous or crystallinity. In the case of cellulose samples, the XRD patterns were recorded in X'Pert PRO PAN analytical instrument operated at 40 kV and AC current of 30 mA with Cu K_{α} radiation at wavelength 0.15406 nm. The diffraction intensities were recorded in the range of $2\theta = 0-80^{\circ}$. The average size of the cellulose particles was calculated using the Scherrer equation [25]:

$$d = \frac{k\lambda}{\beta \cos\theta} \quad (1)$$

where:

- d diameter of the particle
- k constant
- λ wavelength of X-ray radiation

Table 1 Sample codes

Sample characteristics	Sample code
Untreated dry bagasse	DB
Alkali-treated bagasse	ADB
Delignification time (h)	
1	C1
1.5	C1.5
2	C2
2.5	C2.5
3	C3
3.5	C3.5
4	C4

- β full width half maxima (FWHM)
- θ Bragg's diffraction angle

The crystalline index (CI) is another parameter which was calculated using the Segal equation [57]:

$$\frac{I_c - I_a}{I_c} \times 100\% \quad (2)$$

where:

- I_c intensity of peak due to crystalline region
- I_a intensity of peak due to amorphous region

2.3.3 Degree of crystallinity

More commonly, approximately, calibrated methods of measuring crystallinity, W_c , are employed where:

$$W_c = I_c / (I_c + KI_a) \quad (3)$$

where $K = 0.884$ and the range of intensities is $10-32^{\circ}$ in 2θ [21].

2.3.4 Particle size analysis by dynamic light scattering method

The DLS analysis measures the size distribution of the molecules of the sample. The aqueous solution of the cellulose samples were analyzed using DLS analyzer model number MAL1032012 by Malvern, UK.

2.3.5 UV-Vis spectroscopy analysis

The UV-Vis spectroscopy was used to measure the transparency of the sample. The cellulose samples were analyzed using UV-2401 PC UV-Vis recording spectrophotometer by Shimadzu, Japan, in the range of wavelength 200–600 nm with respect to water.

2.3.6 Polarizing light microscope study

The cellulose samples were also observed under the optical image analyzer model number Leica DMLM by Leica, Germany, with both dark field and polarized light effect.

2.3.7 FESEM study

The cellulose samples were analyzed by FESEM model number JEOL JSM-7600F by JEOL, USA, with thermal field emission gun source of ZrO-W.

2.3.8 AFM study

An AFM instrument model number N9410S by Keysight Technologies, USA, was used to scan the specimen surface using contact mode image analysis. One drop of solution was taken on $1\text{ cm} \times 1\text{ cm}$ square of freshly cleaved glass slide, and then the sample was dried under vacuum. The glass slides were blown by nitrogen gas under 0.1% relative humidity condition. An Al-coated Si-cantilever was used in this case.

3 Results and discussions

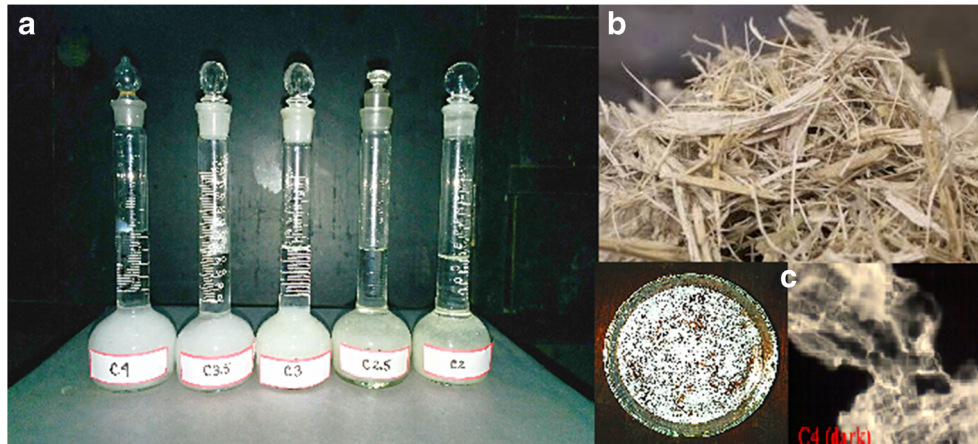
Raw bagasse has light brown hue due to presence of low amount of lignin [26]. With advancement of delignification process, the cellulose appeared white after 1.5-h treatment, and the treated solution did not contain any color. From C2 to C4, the transparency also decreased may be due to size reduction. However this is strictly visual evidence and presented in Fig. 1.

The changes in chemical structure during the whole tenure of the chemical treatment can be predicted from the shifting of IR peaks that correspond to the different functional groups as shown in Fig. 2a–d and tabulated in Table 2. The peak for –OH stretching vibration around 3408 cm^{-1} has been shifted towards higher value indicating the change associated with removal of hemicellulose and generation of free –OH groups. Furthermore, the absorbance value for the peak at 3440 to 3000 cm^{-1} has been increased in the entire treated sample indicating increase in number of free hydroxyl groups. It is maximum for ADB and C1 and then lowered with the others. It has also been reported earlier that with bleaching and alkali treatment, an increase of free hydroxyls of cellulose takes place due to continuous loss of noncellulosic material, higher defibrillation, and fiber opening [20] which further has an impact to further cellulose extraction [49, 60]. With prolonged treatment, reorientation and recrystallization of cellulose further lowered the intensity of the peak though it is still higher

than the DB sample. There is a higher shift of the peak at 3408 cm^{-1} for DB towards around 3440 cm^{-1} indicating lesser degree of hydrogen bonding. The peak around 2900 cm^{-1} for –C–H stretching vibration is continuously shifted towards left indicating continuous removal of noncellulosic hemicellulose and lignin by the total course of treatment. The peak at around 1730 cm^{-1} corresponds to the $>\text{C}=\text{O}$ stretching vibration of acetyl groups of hemicellulose. Absence of the peak from IR spectra of each sample other than the DB indicates removal of the hemicellulose fraction [5]. The peak 1625 cm^{-1} in DB sample indicates the bending mode of absorbed water which after alkali and chlorite treatment changes to 1641 cm^{-1} , i.e., a higher shift indicating higher amount of absorbed water with increasing free hydroxyl group. The peak at 1601.39 cm^{-1} and 1508.88 cm^{-1} corresponds to $>\text{C}=\text{C}$ stretching vibration in lignin aromatic ring, and 1255.56 cm^{-1} signifies –C–O out-of-plane stretching vibration of aryl group in lignin. The relative intensities of those peaks are decreased continuously and removed with the alkali treatment and chlorite treatment, completely removed from C2 sample presenting the evidence of lignin removal [68].

The peak at around 1165 cm^{-1} is responsible for anti-symmetric bridge C–O–C stretching and has been shifted towards 1152 cm^{-1} for C2 sample onwards with different treatments. The continuous reduction in the intensity of the peak indicates the purity of the cellulose extracted from the sugarcane sample [16]. During the total course of treatments, the peak around 1050 cm^{-1} corresponding to C–O/C–C stretching vibration has undergone a lower shift which may be due to change in molecular orientation of cellulose chains caused by different treatments [14]. The peak at 894.44 cm^{-1} corresponds to the rotation of β -glucosidic linkage in cellulose, shifted to slightly higher wavelength indicating transformation of cellulose polymorph by treatments [56]. Simultaneously the small peak observed in DB at 829.17 cm^{-1} for the rotation of β -glucosidic linkage in cellulose is eliminated in ADB which may also be attributed to the abovementioned reason. Out-of-plane bending vibration of

Fig. 1 Image of bagasse sample



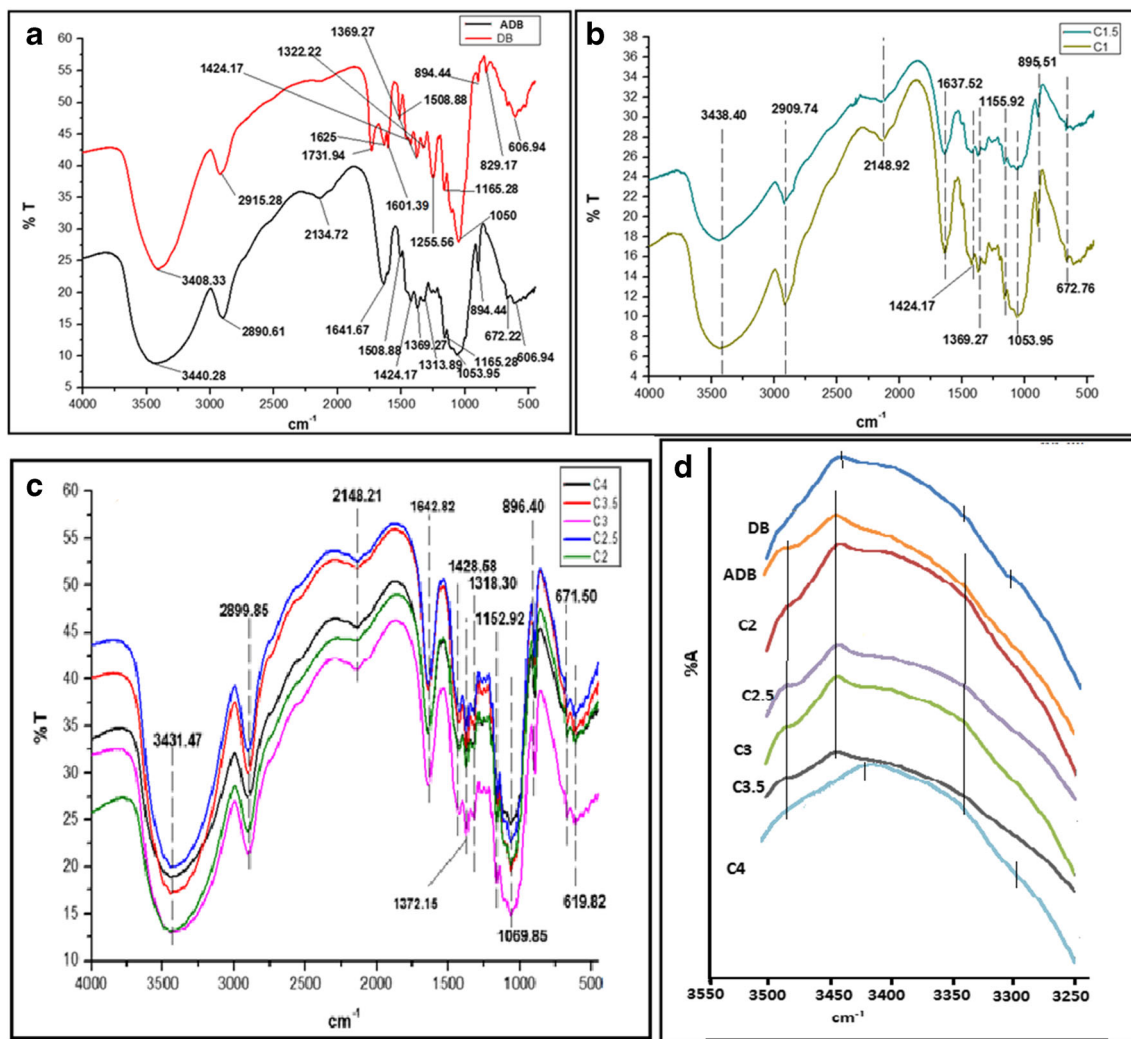


Fig. 2 IR spectra of (a) ADB and DB. (b) C1 and C1.5, (c) C2 to C4, and (d) absorption spectrum of samples in the range of 3250–3550 cm^{-1}

intermolecular hydrogen bonded –OH groups can be identified by the presence of the peak around 670 cm^{-1} , whereas the torsional vibration of the pyranose ring is indicated by the peak at 606.94 cm^{-1} [22, 45, 66]. The higher shift of the peak

at around 607 cm^{-1} may be attributed to the conformational change of cellulose due to removal of noncellulosic material.

The peak position of C2 to C4 in the region 4000 to 3000 cm^{-1} is almost same but further investigated to monitor the fine dilemma obtained for different H-bonding tracing (Fig. 2d). The intramolecular hydrogen bonding of $\text{O}(2)\text{H}—\text{O}(6)$ and $\text{O}(3)\text{HO}(5)$ and the intermolecular hydrogen bonding of $\text{O}(6)\text{H}—\text{O}(3)$ in cellulose are generally shown at $3460–3410$, $3375–3340$, and $3310–3230 \text{ cm}^{-1}$, respectively [46]. For dry bagasses, the corresponding peaks were traced at 3447 cm^{-1} , 3336 cm^{-1} , and 3295 cm^{-1} , respectively. After treatment the peak at 3447 cm^{-1} has been shifted to slightly lower region at around 3436 cm^{-1} up to C3.5 and at around 3425 cm^{-1} for C4 sample. The low peak at 3336 cm^{-1} for DB is also showing low stretching at more or less same region for all the sample responsible for the intramolecular hydrogen bonding of $\text{O}(3)\text{H}—\text{O}(5)$. The peak at 3295 cm^{-1} for $\text{O}(3)\text{H}—\text{O}(6)$ intermolecular H-bonding [32] is also prominent in C4 sample. In alkaline medium, the hydrogen bond of

Table 2 Different parameters from FTIR analysis

Sample	HBI	LOI	TCI
DB	0.6197	0.4998	0.3562
ADB	0.5323	0.4398	0.3639
C1	0.5437	0.4360	0.3371
C1.5	0.5019	0.4285	0.3333
C2	0.5247	0.4210	0.3218
C2.5	0.5399	0.4275	0.3409
C3	0.5703	0.4365	0.3525
C3.5	0.5893	0.4371	0.3601
C4	0.6197	0.4374	0.3695

native cellulose opens forming sodacellulose with high swelling. Upon washing with distilled water and subsequent neutralization by sulfuric acid, there will be regeneration of cellulose molecule leading change in the direction of hydrogen atom in $-OH$ group. This regeneration of cellulose transforms cellulose I to cellulose II to the extent depending on concentration of alkali treatment [14]. This is also evident by the peak at 3482 cm^{-1} for cellulose II starting from ADB to the subsequent sample. There is reduction in LOI value just after alkali treatment (Table 3). LOI is related to the peak at around 1420 cm^{-1} which is attributed to CH_2 symmetric bending or scissoring motion. The ratio of $1424\text{ cm}^{-1}/893\text{ cm}^{-1}$ or LOI indicates the evidence of cellulose I in the cellulosic sample [33]. Decrease in its magnitude in case of ADB indicates conversion of cellulose I to cellulose II, and this decrease continues up to C2 sample and then again increases up to C4 sample but not higher than the DB. Similar observation has also been confirmed by Kumar et al. [34] where LOI of bagasse has been lowered after chemical processing than the native bagasse. However, the increase from C2.5 to C4 may be due to removal of amorphous portion of cellulose by chlorite treatment. Xu et al. [68] also reported that chlorite treatment for longer duration may lead to the dissolution of the amorphous portion of cellulose through depolymerization with the breakdown of β -(1,4) bonds between the saccharide units of cellulose in amorphous portion. Dissolution of amorphous region leads to subsequent fibrillation of cellulose fiber which is also evident by polarizing light micrograph. It is also evident from the TCI data (Table 3), represented by the spectral ratio of 1372 cm^{-1} and the strong peak at 2900 cm^{-1} , that alkali treatment renders increased TCI value due to removal of noncellulosic cementing material [14]. After that the decrease trend of TCI value up to sample C2 after alkali treatment indicates removal of lignin material and opening of hydrogen bond between the lignin and cellulosic $-OH$ group showing a decrease in HBI value [69] presented in Table 2. When matrices in between cellulose microfibril aggregates are extracted, cellulose microfibril aggregates may be rearranged. This renders change in crystallinity also. Furthermore, prolonged

chlorite treatment leads removal of lignin as evident by removal of peak for lignin in the FTIR spectra. Then cellulose began to get exposed with continuous dissolution of amorphous cellulose with an increase in crystalline part of cellulose supported by rise in TCI [68]. The size reduction of cellulose by prolonged chlorite treatment is due to reduction of cellulose degree of polymerization through oxidative cleavage of the cellulose chain [26] which is also supported by particle size analysis data. The higher crystallinity and HBI value for C4 sample can be explained due to extreme fibrillation of cellulose fiber by removal of cementing material followed by subsequent rearrangement which renders new intermolecular H-bond formation as evident by a new peak at 3295 cm^{-1} [32, 68]. The compact packing of cellulose chains decreases the chain flexibility.

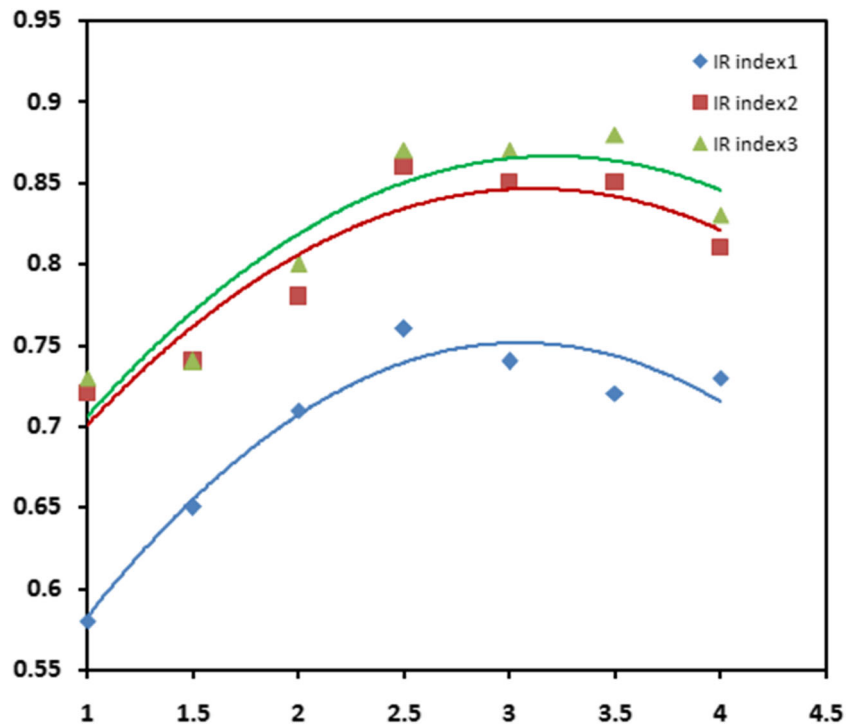
Figure 3 shows the variation of IR index values for C1 to C4 sample with respect to the peak 895 cm^{-1} , 672 cm^{-1} , and 619 cm^{-1} , and the reference peak is 2909 cm^{-1} to predict the change in fine structure of cellulose. In all the three curves, the maxima obtained at around sample C2.5 and then it falls gradually. The intensity change in the 609 cm^{-1} band is influenced by the torsional vibration of pyranose ring. The increase in the value of IR index with the increasing time of chlorite treatment indicates that the removal of cementing material from bamboo allows the pyranose ring to undergo more torsional vibration. The intensity change for the peak 895 cm^{-1} is associated with conformational changes occurring during conversion of cellulose I to cellulose II. It is well known that by alkali treatment, cellulose I converts into cellulose II [14], but the value still changes afterwards. This is probably due to the change in surrounding of the cellulose chains by continuous removal of noncellulosic material with alkali and subsequent chlorite treatment. As those binding materials are getting removed, the cellulose chains are having more free $-OH$ groups and change in amount of crystalline and amorphous cellulose. The pyranose rings are being more strain free [1, 42]. After that there is removal of amorphous cellulose by prolonged chlorite treatment increasing crystalline part and hence restricting the free movement of cellulose molecules rendering decrease in IR index value.

Figure 4 represents XRD data for the chlorite-treated bagasse sample (C2–C4) and for DB and ADB in the insight. In case of dry bagasse sample, a broad peak at around $2\theta = 16.5^\circ$ and 22.5° and 34.6° [34] which are supposed to represent the typical cellulose I structure. The peak at 14.5° is probably merged with 16.5° and appeared as a broad one due to the presence of impurities (such as lignin, hemicelluloses, pectins, and amorphous cellulose) [42, 51]. This is further substantiated by the presence of both peaks after alkali treatment where removal of hemicellulose has been achieved by alkali treatment. It has already discussed in FTIR section. In case of ADB sample, a short peak in between 20 and 21° also confirms the presence of cellulose II. The XRD patterns of all

Table 3 Different parameters obtained from AFM analysis of the cellulose samples

Parameters	Value (for C2)	Value (for C4)	Unit
Root mean square height	8.28	11.6	nm
Skewness	0.118	0.863	
Kurtosis	3.66	7.20	
Maximum peak height	38.8	96.9	nm
Maximum pit height	46.6	54.1	nm
Maximum height	85.5	151	nm
Arithmetic mean height	6.40	8.53	nm

Fig. 3 IR index for C1–C4 samples (1) 895 cm^{-1} , (2) 672 cm^{-1} , and (3) 619 cm^{-1}



chlorite-treated samples exhibited peaks at 2θ around 16.5° , 22.5° , and 35° which were attributed to the planes of (1 1 0), (2 0 0), and (040), respectively, representing that of cellulose I [34]. The diffraction peaks at 2θ around 12.6° corresponding to the (1 1 0) and a mid-shoulder in between 20 and 21° corresponding to (101) plane were signed to cellulose II. It has been established that during alkali treatment, conversion from cellulose I to cellulose II takes place with the extent of conversion depending on degree of alkali treatment [14]. Hence, the XRD peak for all the characterized samples is showing the presence of respective peaks for both cellulose I and cellulose II. Xu et al. [68] reported that with prolonged chlorite treatment, dissolution of the amorphous cellulose took place. That leads overlapping of two closely spaced peaks:

mid-shoulder in between 20° and 21° corresponding to (101) and the highest peak at 22.5° . This may plausibly occur due to change in crystal structure associated with removal of impurities.

XRD data shows a linear trend of crystallinity with a drop after alkali treatment. This means that peak width indicated by full width half maxima (FWHM) due to crystallite size varies inversely with crystallite size as the crystallite size gets smaller, the peak gets broader. The chemical treatment made on sugarcane bagasse in this work renders decrease in FWHM values with parallel increase in crystallite size. As reported by Das and Chakraborty [14] with alkali treatment, cellulose forms sodacellulose first with dissolution noncellulosic material mainly hemicelluloses and then with subsequent

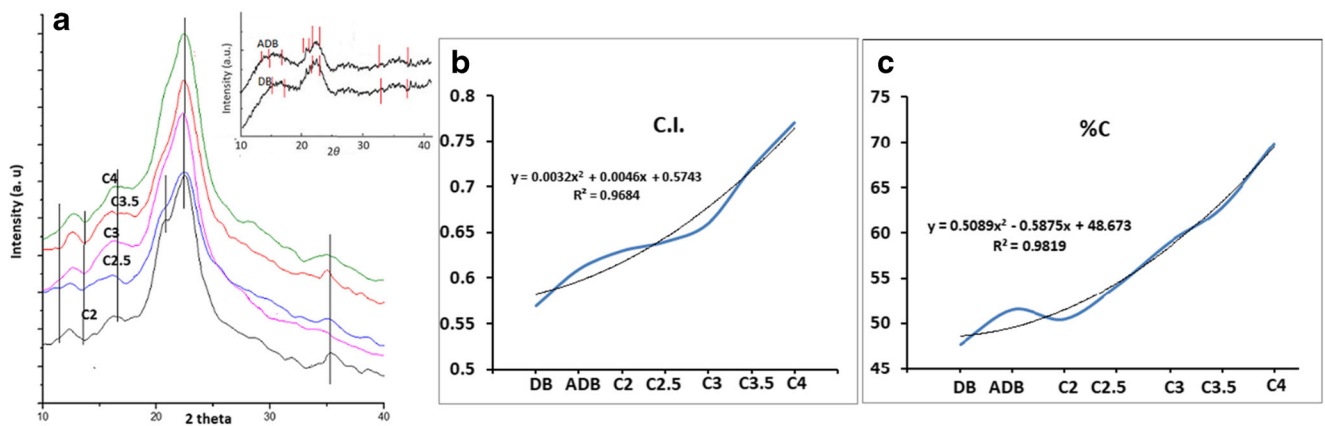
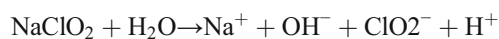


Fig. 4 XRD plot of cellulose samples (a) C2–C4; insight DB and ADB; (b) curve fitting for degree of crystallinity; and (c) curve fitting for percent crystallinity

acidification cellulose regenerates. By this process, opening up of H-bonding takes place along with further recrystallization of cellulose. This is the reason behind the observation of increase in crystallite size along with % crystallinity after alkali treatment [43]. It is evident from FTIR study that with initial chlorite treatment hour, i.e., from C1.5 sample, lignin components are absent. Hence after ADB XRD study has been made with C2–C4 samples. With prolonged chlorite treatment, lignin, hemicelluloses, and other amorphous materials are removed from the fiber bundle [1, 31, 38, 64] initially leading to separation of fibril. It has been reported by Rezende et al. [54] that lignin works as glue among the fibril. Due to this fibrillation, the compact packing of cellulose structure has lost leading to decrease in % crystallinity and crystallite size up to C2 sample. This observation has also been supported by the value of TCI and HBI obtained from FTIR study. Similar observation has been reported by de Carvalho Benini et al. [17] in their work of alkali treatment and subsequent three-stage bleaching of *Imperata brasiliensis* grass. After alkali treatment, there is increase in crystallinity followed by lowering with first stage of bleaching and increase by later stages. After C2 there is increase in % crystallinity due to removal of amorphous cellulose by prolonged chlorite treatment [27, 68]. All these observations are well supported by the similar trend in TCI and HBI value obtained with FTIR study. The highest crystallite size is with C4 sample which possess highest value for HBI, and an intermolecular H-bonding is also observed in this case. Degree of crystallinity indicates the total mass fraction of crystalline portion [55]. The trend of percent crystallinity has been also maintained in case of degree of crystallinity value, and in both the cases, a polynomial curve has fit with a regression value of 0.98 (Fig. 4). Mean orientation angle obtained from the data are also given. This parameter is indicative of spiral angle (the angle at which the fibril spirals around the axis of the fiber). The decrease in orientation angle is resulted from an increased orientation of fibrils with respect to the fiber axis. There is not any marked difference in orientation angle due to all the treatment. Herman's orientation factor f_x is calculated from the mean orientation angle value, and it has been found that f_x value has been increased from 0.9424 to 0.9437. Increase f_x indicates increase in modulus of fiber (Das et al., 2006).

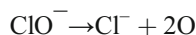
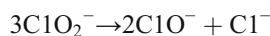
Higginbotham et al. (1962) predicted the presence alternative mechanism without involving chlorine dioxide and chlorous acid. As per the present study, the pH of 2% NaClO₂ solution is around 12 indicating presence of excess hydroxyl ion. As chlorous acid is a weak acid, its dissociation is negligible showing alkaline pH.



The ether group present in lignin undergoes hydrolysis under the influence of hydroxyl ions with dissolution of the

soluble fraction of lignin as presented by the reaction scheme in Fig. 5.

By the continuous reaction of OH⁻ and lignin, the concentration of OH⁻ will decrease continuously shifting the equilibrium towards left by which the solution pH tends towards 8. Then in the medium H⁺ ion concentration increases as evident from the pH shift and probably then the following reactions take place to continue conventional delignification by chlorite under pH at around 8.



The rate of reaction is very slow under this series of pH, but the long duration of time at a temperature of around 80 °C compensates the extent of bleaching.

Figure 6A shows the optical micrograph analysis of cellulose in the view of dark field, and Fig. 6B presents the scanning electron micrograph. From the figure, it can be seen that with an increase in delignification time, the fibrillation is prominent. Natural fibers are by default composite in nature in which cellulose fibers are acting as the reinforcement and embedded in hemicelluloses and lignin matrix with strong inter- and intramolecular H-bonding. Those matrix materials when removed by different chemical treatment, the compact composition of the natural fibers was lost, and due to opening of H-bonding, free –OH groups generation take place [20]. This change in cellulose fibers leads them to smaller unit, fibril by the process of fibrillation [38]. The process of removal of matrix material from the native bagasse and fibrillation is clearly evident from the morphology by PLM and FESEM. The insight SEM picture in B1 and image A1 indicates that initial fiber bundles are tightly bound with noncellulosic materials. The matrix material has been started to dismantle with the alkali treatment (Fig. 6 (B2)) as evident from SEM micrographs, and continuous increase in fibrillation is prominent by the series of chlorite treatment (Fig. 6 (A1–A6 and B3)). A clear separation of fibers is observed from C3 (A5) which are getting finer and finer with higher chlorite concentration rendering more intense fibrillation (A6) [17]. The chemical treatments render roughness in cellulose fiber surface (B4). All these observation substantiate the findings with FTIR and XRD study. Consequently, it can be predicted that the extracted cellulose has higher aspect ratio and surface area which in turn may improve interaction with functionalizing agent and/or fiber–matrix interfacial bonding in case of composites fabrication [38].

The DLS analysis, displayed in Fig. 7, exhibits that as the delignification time is increased, the hydrodynamic diameter of the cellulose colloidal particles is reduced which contradicts with XRD observation. The slight increase of the value for C2.5 is probably due to the intermolecular H-bonding with the

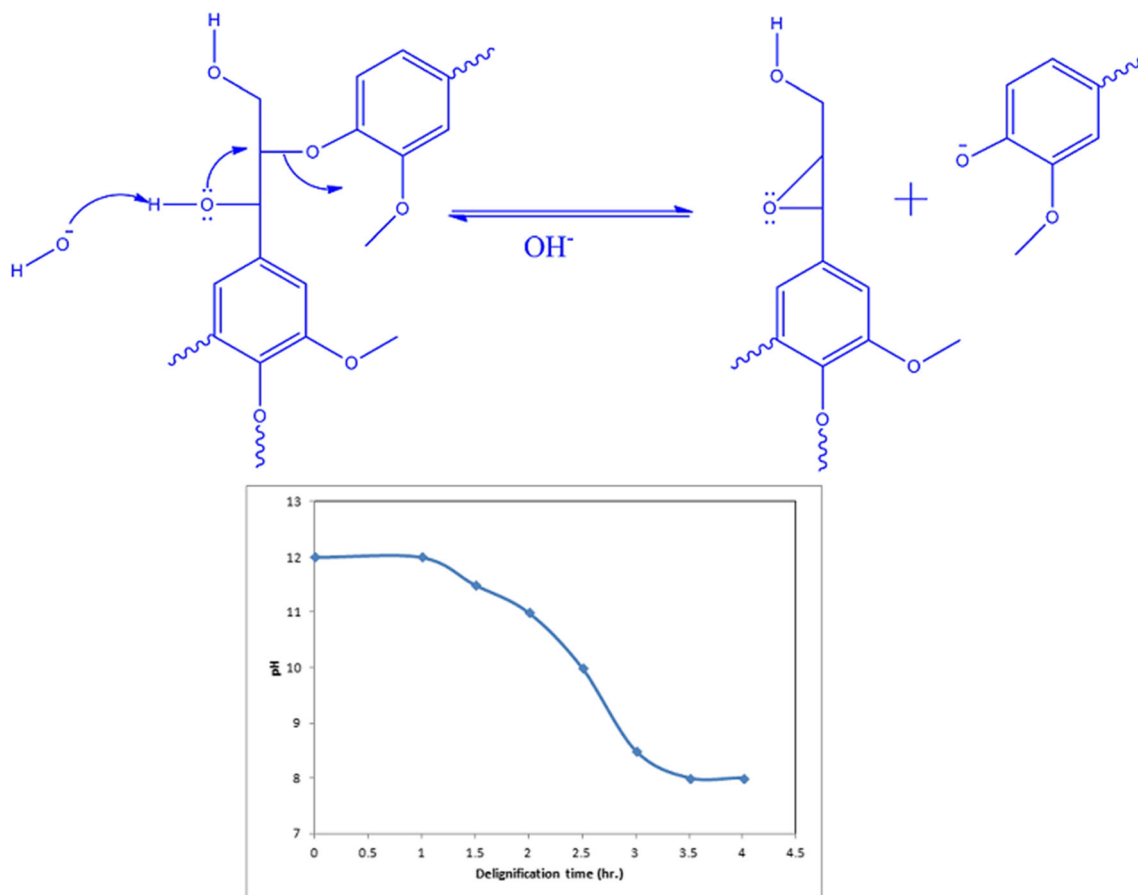


Fig. 5 Reaction scheme for delignification at alkaline pH and plot for change in pH during delignification

absorbed water molecules. The increase in value from C3.5 to C4 is not very significant which indicates the chances of formation of intra-/intersheet H-bonding in C4 which obeys the XRD data also. The polydispersity indices ranged from 0.3 to 0.6, which measures the broadness of the size distribution. Colloid with an index value below 0.05 is monodisperse, below 0.08 is nearly monodisperse, 0.08–0.7 is midrange value, and above 0.7 is a broad distribution [6]. The PDI value illustrates that the C2 and C4 are highly monodispersed, whereas sample C3.5 shows highest polydispersity in particle size dispersion of particles in colloidal state. From the DLS curves and the peak intensities, it can also be predicted that the particle size in water is continuously reducing from C2 onwards and more or less same for C3.5 and C4. The crystallinity of C2 is lower than the subsequent samples containing higher amount of free –OH group as evident from lower HBI value, and the optical microscope image shows that the fiber is not too much free from amorphous material. These impurities and free –OH group will help them to agglomerate easily and will be hydrated in a larger size particle very easily [18]. The zeta potential value also indicates the stability of the agglomerates. Due to this agglomeration and hydration, they are stabilized forming larger particle of uniform distribution indicated by the PDI value. With prolonged chlorite treatment, the amorphous

portion of cellulose is continuously being removed indicated by decreasing size of radius of hydration. It has been observed that with removal of amorphous material, the polydispersity is showing a large variation indicating a distribution of particle size. With change in fibrillation of fiber as evident from microscopic image the particle and increasing crystallinity, they have shapes which are devoid of spherical nature. During Brownian motion of the colloidal suspension, the different cellulose sample particles are capturing themselves giving rise to particles or clusters of wide size distribution [19]. This has been established further by increase in PDI value and zeta potential value indicating different agglomerating tendency. In case of the highest crystalline sample C4 with removal of maximum amount of amorphous portion and extreme fibrillation, the particles are again showing monodispersity. The greater the value of ζ -potential, the greater will be the colloidal stability. Usually a value less than –15 mV indicates the onset of agglomeration, while the values greater than –30 mV generally represents that the colloidal dispersion is stable with sufficient mutual repulsion [70]. In this case, the range of ζ -potential is not showing high stability or high tendency to agglomerate presenting a linear decreasing trend.

Figure 8 shows the surface morphology of C2 and C4 by AFM. From Table 3, it can be clearly seen that both the

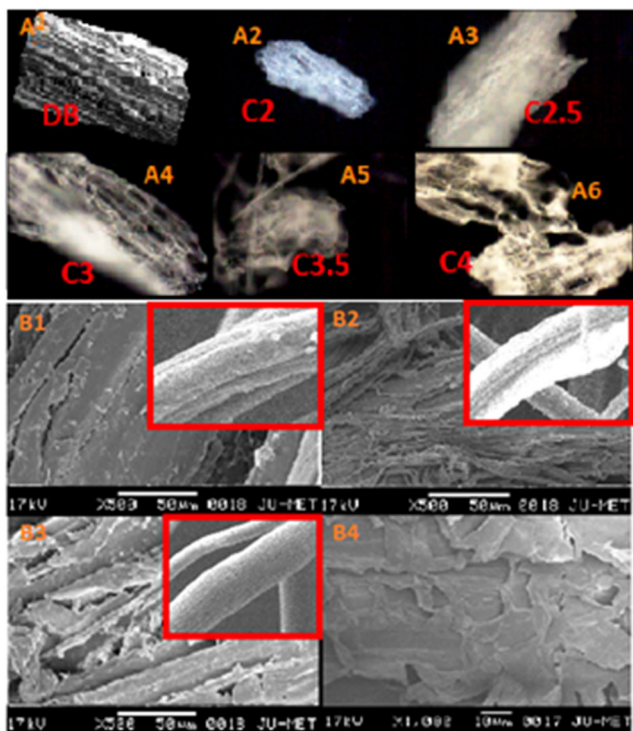
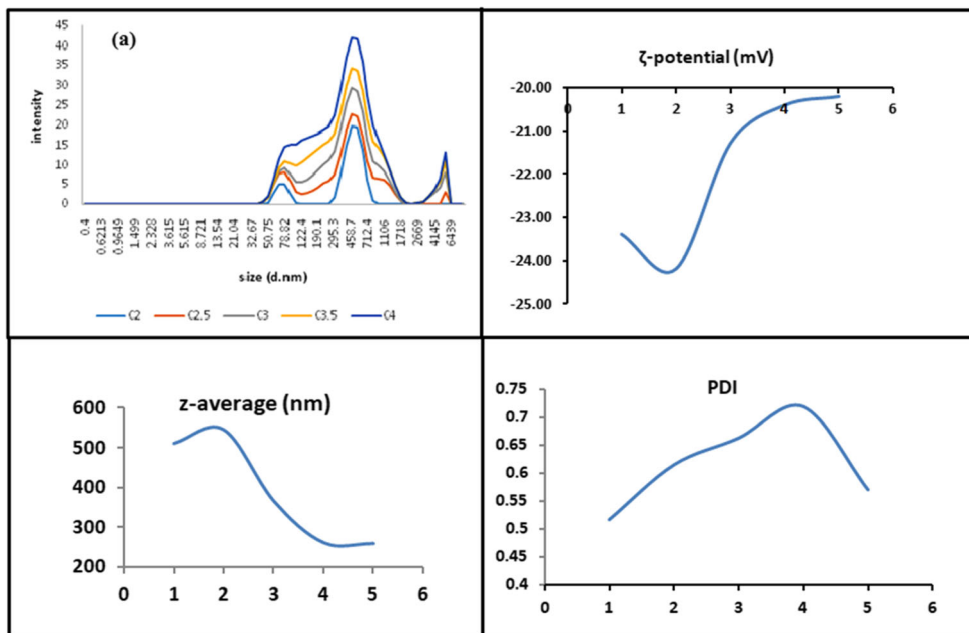


Fig. 6 A1–A6, dark field optical micrographs of different samples (magnification $\times 25$). Sem micrographs: B1, untreated bagasse; B2, alkali-treated bagasse; B3, alkali and 4-h chlorite-treated bagasse (C4); B4, magnified view of C4 (all insight magnification $\times 1000$, $10 \mu\text{m}$)

skewness and kurtosis of C4 are greater than the C2 which denotes the difference of the number of peaks and number of valleys as well as the difference between the number of pits and number of peaks of C4 which is greater than the C2.

Skewness (Ssk) is a measure of the distribution of roughness shape relative to the mean (asperity). If Ssk has value greater than zero, it indicates a surface dominated by peaks and less than zero means a surface with pits or valleys (ISO 25178). Here the value of Ssk is greater than zero in both the cases which indicates that there are peaks present in the surface, whereas the higher value of C4 indicates higher number of peaks in the surface. The surface topography presented in Fig. 6 also exhibits the same fact. In case of topography, the phase is identified with color, i.e., dark is low and bright is high [23]. The C4 topography is identified with brighter phase than C2, and similarly in phase profile, there is more uniformity in brighter phase. The higher amount of bright phase in C4 indicates higher crystalline portion, whereas more dark regions in C2 is for the presence of higher amount of amorphous portion [35, 65]. Kurtosis (Sku) is a measure of the sharpness of the roughness profile. Sku value greater than three indicates especially spike-like features, Sku equal to three implies a normally distributed surface, and Sku less than three indicates height distribution which is skewed above the main plane (ISO 25178). The value for Sku for C2 and C4 is 3.66 and 7.20, respectively, indicating higher concentration of spike-like feature in the surface. This result further established the increase in crystallinity in C4 and dissolution of amorphous phase as evident from FTIR and XRD study. Chen et al. [11] reported that during AFM study in contact mode, amorphous alloys can generate a few deep pits, while crystalline alloys may have both deep and shallow pits. The comparison of line profile for both the sample also indicate higher amount of pit in C4 sample indicating higher crystallinity in the sample. The peak height of C4 is higher than C2 indicating higher crystallite

Fig. 7 DLS plot of the cellulose samples



1: C2, 2: C2.5, 3: C3, 4: C3.5, 5: C4

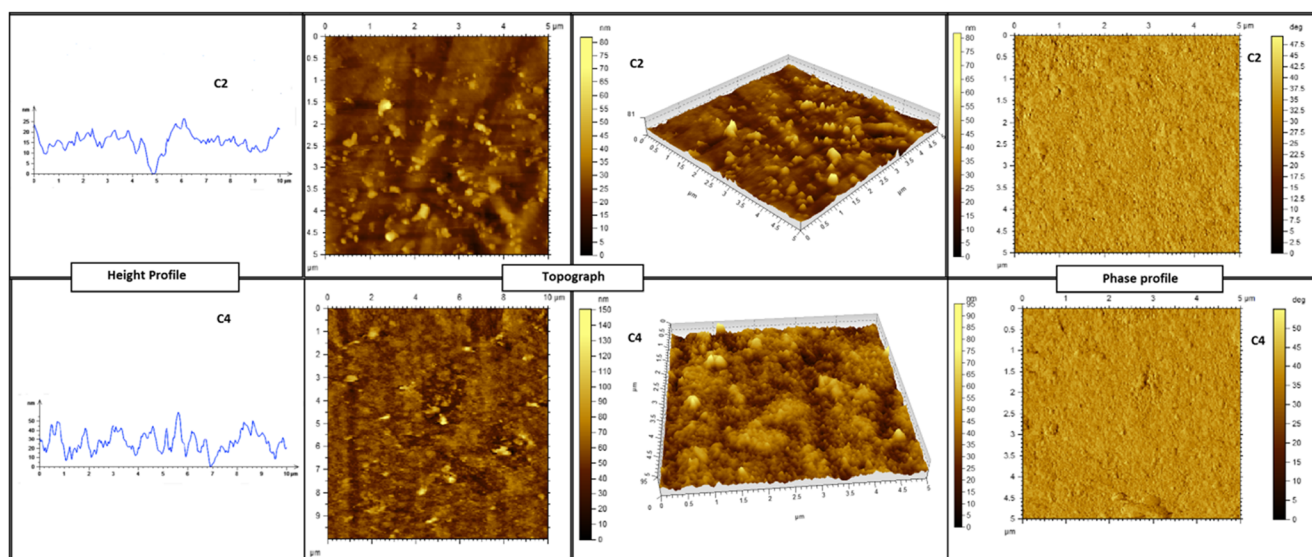


Fig. 8 AFM surface morphology of C2 and C4 cellulose samples

size which is also supported by XRD study. The higher peak height for C4 is again substantiating the existence of intersheet H-bonding in case of C4 in FTIR spectra. The root mean square height, S_q , represents the standard deviation of height which is also higher for C4. The arithmetic mean height S_a , measure of surface roughness parameter, is 6.40 and 8.53 for C2 and C4 sample, respectively. This result also predicts that removal of noncellulosic cementing material and amorphous material from the bagasse fiber increases the surface roughness continuously. Similar observation is obtained with SEM and optical microscope study. From the optical microscope image, it is clear that fibers are fibrillated, i.e., form a loosely adhered fibrillar network, but not separated into nanocrystalline form. This is very much clear from AFM topograph. Comparing C2 and C4 topograph and phase profile, it is clear that the cementing material is higher in concentration while in C4 higher surface roughness removing more amorphous cellulose with clear observation of fibrillation. The average fibril diameter obtained from height profile of C4 varies within $0.2 \pm 0.1 \mu\text{m}$ ($200 \pm 100 \text{ nm}$) which is $0.5 \pm 0.2 \mu\text{m}$ ($500 \pm 200 \text{ nm}$) for C2. The more uneven nature of height profile for C4 indicates the surface roughness and fibrillated network. The lowering of diameter of cellulose fiber for C4 indicates increase in aspect ratio by prolonged chlorite treatment under alkaline pH.

It has been reported by Barbosa et al. [3] that carbonyl and carboxyl groups are important components of bleached lignocellulosic material as during dissolution of amorphous cellulose by acid chlorite treatment oxidative cleavage of cellulose chain takes place [68]. Figure 9 shows UV-Vis absorbance spectra of the cellulose samples against wavelength showing a maximum absorbance near the wavelength 266 nm for all the cellulose samples. It has been reported by Bos [7] that the acetal linkage is not responsible for the absorption peak at 260 nm, but rather the ketonic carbonyl groups are supposed

to be responsible for this peak. The C4 shows the maximum absorbance with a distinct peak indicating highest concentration of the carbonyl group due to longer time of exposure with chlorite treatment. It has the lowest transparency among the cellulose samples. This fact is also supported by the visual evidence of transparency evident from Fig. 1. From XRD study, the largest crystallite size is also obtained with C4 sample, and the transparency of a sample is inversely proportional to crystallite size as the light scatter more with larger crystallite instead of passing through.

Figure 10 represents the TGA plots of the dry bagasse, ADB, C2, and C3.5. The thermal decomposition of all the samples consists of three decomposition zone.

The first decomposition zone indicates loss of moisture (from 30 to 70 °C) which is adsorbed or attached to the cellulose molecule or other noncellulosic material by intermolecular H-bonding. The order of crystallinity for the samples varies as

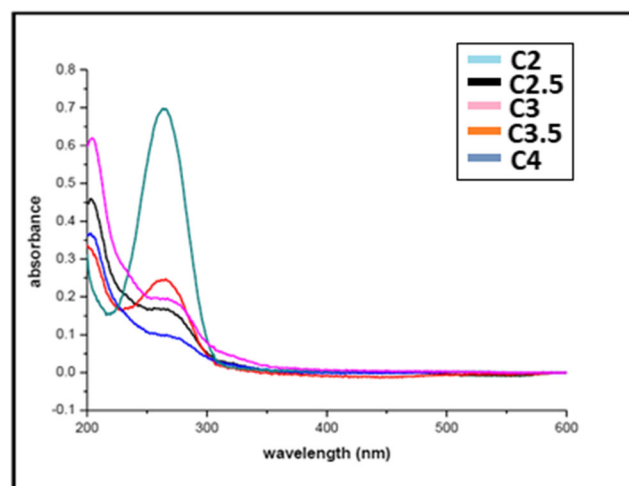


Fig. 9 UV-Vis spectroscopy plot of cellulose samples

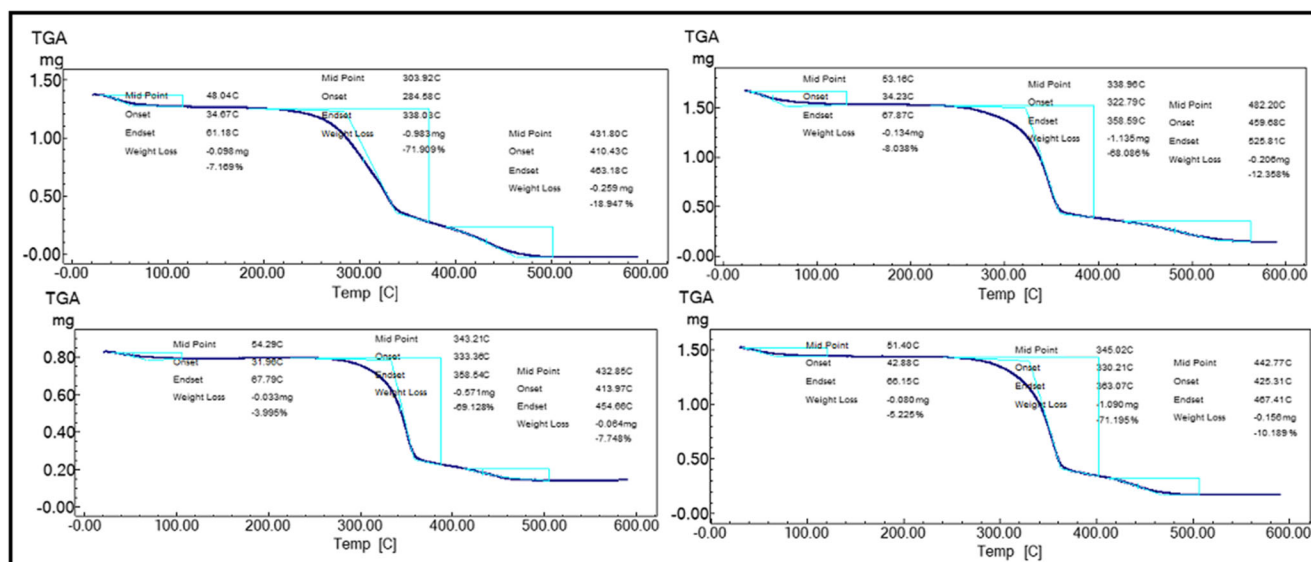


Fig. 10 TGA plot of the cellulose samples

DB<ADB>C2<C4; hence, the temperature for maximum amount of water loss follows the same trend due to tight packing of structure with increase crystallinity of cellulose. It is also observed from the data that bound water is present in highest amount in case of ADB due to presence of free –OH group by removal of hemicelluloses and lignin. However, the amount is decreasing with increase in cellulose crystallinity and removal of cementing material with other treated samples. From C2 to C4, the amount of adsorbed moisture is higher because with extreme fibrillation of C4, the surface area of fiber increased [1]. This factor prevails over crystallinity resulting in the higher amount of adsorbed water [9].

The second region corresponds to cellulose rather than hemicellulose as mentioned in thermal study of natural fibers by other workers [4, 15, 53]. Natural fiber itself is composite in nature, and merged degradation may be observed due to integrated binding of cellulose fiber with other noncellulosic material [15]. The peak for DB is at 322 °C which has been shifted to 285 °C for ADB and showing continuous increase to 333.36 °C for C2 sample and ends within 370 °C for C4. The lowering of peak for ADB may be attributed to the removal of hemicelluloses (as evident from FTIR study), generation of free –OH group, and destruction of composite structure of the bagasse fiber itself. With prolonged chlorite treatment, the fiber resembles crystalline cellulose more approaching the degradation peak of α cellulose [15, 41]. All the chlorite-treated samples are showing better stability with respect to the degradation temperature due to higher crystallinity of cellulose leading to better packing of cellulose chains. Another fact is also evident from the amount of degradation that with higher chemical treatment, amount of cellulose is also increasing. The final decomposition (from 410 to 470 °C) indicates char oxidation of cellulose samples [12]. It is observed that with respect to percent weight loss, dry bagasse shows highest amount as along with

charring of cellulose the cementing material present in dry bagasse will also undergo decomposition at this higher temperature. Considering the percent residual weight, it can be predicted that any treatment increase thermal stability of cellulose sample. From sample C2 to C4, the thermal stability lowered to some extent as this sample suffers more fibrillation of cellulose with higher surface area and more susceptible to thermal degradation.

4 Conclusion

Alkali treatment and chlorite treatment of sugarcane bagasse alter the fine structure to a great extent. Delignification of bagasse with sodium chlorite in alkaline medium to highly fibrillated cellulose fiber with variation of treatment time is a novel study carried out by present investigators. FTIR and XRD study revealed that alkali treatment and lignin treatment up to 1.5 h successfully removed the noncellulosic binding material of bagasse and prolonged chlorite treatment up to 4 h further removed the amorphous portion of cellulose rendering increase in crystallinity. However, chlorite treatment was not carried out for further duration as the sample suspension lose a high degree of transparency which is further established by sharp UV peak, radius of hydration obtained in consecutive two samples is more or less the same. The best sample of extracted cellulose is with high crystallinity with dimension of 259.3 nm and PDI of 0.57. AFM study also established extraction of highly crystalline cellulose particles with removal of noncellulosic and amorphous cementing material from bagasse with enhanced surface roughness and aspect ratio. Thermal stability of the sample is nearly similar for ADB and C2 sample while considering the residual weight. However, this is reduced with prolonged chlorite treatment

due to increase of surface area of fiber by excessive fibrillation. This highly fibrillated cellulose fiber possesses high aspect ratio and larger surface area which make them suitable as reinforcing agent for biocomposite with a good interfacial adhesion with matrix.

Supplementary Information The online version contains supplementary material available at <https://doi.org/10.1007/s13399-020-01120-2>.

References

- Ahmad R, Hamid R, Osman SA (2019) Physical and chemical modifications of plant fibres for reinforcement in cementitious composites. *Adv Civ Eng* 2019. <https://doi.org/10.1155/2019/5185806>
- Balakrishnan P, Sreekala MS, Kunaver M, Huskić M, Thomas S (2017) Morphology, transport characteristics and viscoelastic polymer chain confinement in nanocomposites based on thermoplastic potato starch and cellulose nanofibers from pineapple leaf. *Carbohydr Polym* 169:176–188. <https://doi.org/10.1016/j.carbpol.2017.04.017>
- Barbosa LCA, Maltha CRA, Demuner AJ et al (2013) A rapid method for quantification of carboxyl groups in cellulose pulp. *Bioresources* 8:1043–1054. <https://doi.org/10.15376/biores.8.1.1043-1054>
- Basak RK, Saha SG, Sarkar AK, Saha M, Das NN, Mukherjee AK (1993) Thermal properties of jute constituents and flame retardant jute fabrics. *Text Res J* 63:658–666. <https://doi.org/10.1177/004051759306301107>
- Beck-Candanedo S, Roman M, Gray DG (2005) Effect of reaction conditions on the properties and behavior of wood cellulose nanocrystal suspensions. *Biomacromolecules* 6:1048–1054. <https://doi.org/10.1021/bm049300p>
- Beyene D, Chae M, Dai J, Danumah C, Tosto F, Demesa AG, Bressler DC (2018) Characterization of cellulase-treated fibers and resulting cellulose nanocrystals generated through acid hydrolysis. *Materials* 11:1272–1283. <https://doi.org/10.3390/ma11081272>
- Bos A (1972) The UV spectra of cellulose and some model compounds. *J App Polym Sci* 16:2567–2576. <https://doi.org/10.1002/app.1972.070161010>
- Brinchi L, Contana F, Fortunati E, Kenny JM (2013) Production of nanocrystalline cellulose from lignocellulosic biomass: technology and applications. *Carbohydr Polym* 94:154–169. <https://doi.org/10.1016/j.carbpol.2013.01.033>
- Cabrales L, Abidi N (2019) Kinetics of cellulose deposition in developing cotton fibers studied by thermogravimetric analysis. *Fibers* 7:78–83. <https://doi.org/10.3390/fib7090078>
- Camani PH, Anholon BF, Toder RR, Rosa DS (2020) Microwave-assisted pretreatment of eucalyptus waste to obtain cellulose fibers. *Cellulose* 27:3591–3609. <https://doi.org/10.1007/s10570-020-03019-7>
- Chen H, Qin Z, He M, Liu Y, Wu Z (2020) Application of electrochemical atomic force microscopy (EC-AFM) in the corrosion study of metallic materials. *Materials* 13:668. <https://doi.org/10.3390/ma13030668>
- Ching YC, Tuck SN (2014) Effect of preparation conditions of cellulose from oil palm empty fruit bunch fiber. *BioRes*. 9:6373–6385
- Csiszár E, Nagy S (2017) A comparative study on cellulose nanocrystals extracted from bleached cotton and flax and used for casting films with glycerol and sorbitol plasticisers. *Carbohydr Polym* 174:740–749. <https://doi.org/10.1016/j.carbpol.2017.06.103>
- Das M, Chakraborty D (2006) Influence of alkali treatment on the fine structure and morphology of bamboo fibers. *J Appl Polym Sci* 102:5050–5056. <https://doi.org/10.1002/app.25105>
- Das M, Chakraborty D (2008) Thermogravimetric analysis and weathering study by water immersion of alkali-treated bamboostrips. *BioRes* 3:1051–1062
- de Assis ACL, Alves LP, Malheiro JPT et al (2019) *Opuntia Ficus-Indica* L. Miller (Palma Forrageira) as an alternative source of cellulose for production of pharmaceutical dosage forms and biomaterials: extraction and characterization. *Polymers* 11:1124. <https://doi.org/10.3390/polym11071124>
- de Carvalho Benini KC, Ornaghi HL, Pereira PH, Maschio LJ, Voorwald HJ, Cioffi MO (2020) Survey on chemical, physical, and thermal prediction behaviors for sequential chemical treatments used to obtain cellulose from *Imperata Brasiliensis*. *J Therm Anal Calorim*. <https://doi.org/10.1007/s10973-019-09221-5>
- de Souza AG, Barbosa RFS, Rosa DS (2020) Nanocellulose from industrial and agricultural waste for further use in PLA composites. *J Polym Environ* 28:1851–1868. <https://doi.org/10.1007/s10924-020-01731-w>
- de Souza AG, de Lima GF, Colombo R, Rosa DS (2020) A new approach for the use of anionic surfactants: nanocellulose modification and development of biodegradable nanocomposites. *Cellulose* 27:5707–5728. <https://doi.org/10.1007/s10570-020-03160-3>
- Ferreira FV, Mariano M, Rabelo SC, Gouveia RF, Lona LMF (2018) Isolation and surface modification of cellulose nanocrystals from sugarcane bagasse waste: From a micro- to nano-scale view. *Appl Surf Sci* 436:1113–1122. <https://doi.org/10.1016/j.ap.susc.2017.12.137>
- Fischer EW, Lorenz R (1963) über Fehlordnungen in Polyäthylen-Einkristallen. *Kolloid-Zeitschrift und Zeitschrift für Polymere* 189(2):97–110
- Garside P, Wyeth P (2013) Identification of cellulosic fibres by fur spectroscopy – thread and single fibre analysis by attenuated total reflectance. *Stud Conserv* 48:269–275. <https://doi.org/10.1179/sic.2003.48.4.269>
- Haugsted G (2012) Atomic force microscopy: understanding basic modes and advanced applications. John Wiley & Sons, Inc., Hoboken
- Higginbotham RS, Leigh RA (1962) Bleaching of cotton with sodium chlorite. *J Text Inst* 53:312–319. <https://doi.org/10.1080/19447016208688724>
- Holzwarth U, Gibson N (2011) The Scherrer equation versus the Debye-Scherrer equation. *Nat Nanotechnol* 6:538. <https://doi.org/10.1038/nnano.2011.145>
- Hubbell CA, Ragauskas A (2010) Effect of acid-chlorite delignification on cellulose degree of polymerization. *Bioresour Technol* 101:7410–7415. <https://doi.org/10.1016/j.biortech.2010.04.029>
- Gan I, Chow WS (2019) Tailoring chemical, physical, and morphological properties of sugarcane bagasse cellulose nanocrystals via phosphorylation method. *J Nat Fibers*. <https://doi.org/10.1080/15440478.2019.1691120>
- Jonoobi M, Oladi R, Davoudpour Y, Oksman K, Dufresne A, Hamzeh Y, Davoodi R (2015) Different preparation methods and properties of nanostructured cellulose from various natural resources and residues: a review. *Cellulose* 22:935–969. <https://doi.org/10.1007/s10570-015-0551-0>
- Kallel F, Beltaieb F, Khiari R, García A, Bras J, Chaabouni SE (2016) Isolation and structural characterization of cellulose nanocrystals extracted from garlic straw residues. *Ind Crop Prod* 87:287–296. <https://doi.org/10.1016/j.indcrop.2016.04.060>

30. Kargarzadeh H, Mariano M, Gopakumar D, Ahmad I, Thomas S, Dufresne A, Huang J, Lin N (2018) Advances in cellulose nanomaterials. *Cellulose* 25:2151–2189. <https://doi.org/10.1007/s10570-018-1723-5>
31. Kassab Z, Kassem I, Hannache H, Bouhfid R, El Achaby M (2020) Tomato plant residue as new renewable source for cellulose production: extraction of cellulose nanocrystals with different surface functionalities. *Cellulose* 27:4287–4303. <https://doi.org/10.1007/s10570-020-03097-7>
32. Kondo T (1997) The assignment of IR absorption bands due to free hydroxyl groups in cellulose. *Cellulose* 4:281–292. <https://doi.org/10.1023/A:1018448109214>
33. Kumar A, Negi S, Choudhary V, Bhardwaj NK (2012) Synthesis and characterization of methylcellulose/PVA based porous composite. *Carbohydr Polym* 88:1364–1372. <https://doi.org/10.1016/j.carbpol.2012.02.019>
34. Kumar A, Negi YS, Choudhary V, Bhardwaj NK (2014) Characterization of cellulose nanocrystals produced by acid-hydrolysis from sugarcane bagasse as agro-waste. *J Mater Phys Chem* 2:1–8. https://doi.org/10.1007/978-3-642-27758-0_1162-2
35. Lahiji RR, Xu X, Reifemberger R, Raman A, Rudie A, Moon RJ (2010) Atomic force microscopy characterization of cellulose nanocrystals. *Langmuir* 26:4480–4488. <https://doi.org/10.1021/la903111j>
36. Lam NT, Chollakup R, Smitthipong W, Nimchua T, Sukyai P (2017) Utilizing cellulose from sugarcane bagasse mixed with poly(vinyl alcohol) for tissue engineering scaffold fabrication. *Ind Crop Prod* 100:183–197. <https://doi.org/10.1016/j.indcrop.2017.02.031>
37. Lamaming J, Hashim R, Leh CP, Sulaiman O (2017) Properties of cellulose nanocrystals from oil palm trunk isolated by total chlorine free method. *Carbohydr Polym* 156:409–416. <https://doi.org/10.1016/j.carbpol.2016.09.053>
38. Lazić BD, Janjić SD, Rijavec T, Kostić M (2017) Effect of chemical treatments on the chemical composition and properties of flax fibers. *J Serb Chem Soc* 82:83–97. <https://doi.org/10.2298/JSC16070716L>
39. Ma'ruf A, Pramudono B, Aryanti N (2017) Lignin isolation process from rice husk by alkaline hydrogen peroxide: lignin and silica extracted. *AIP Conference Proceedings* 1823:020013. <https://doi.org/10.1063/1.4978086>
40. Mishra SP (2010) A text book of fibre science & tech. New age international (P) limited, Delhi
41. Mohomane SM, Motaung TE, Revaprasadu N (2017) Thermal degradation kinetics of sugarcane bagasse and soft wood cellulose. *Materials* 10:1246. <https://doi.org/10.3390/ma10111246>
42. Mondragon G, Fernandes S, Retegi A, Peña C, Algar I, Eceiza A, Arbelaiz A (2014) A common strategy to extracting cellulose nanoentities from different plants. *Ind Crop Prod* 55:140–148. <https://doi.org/10.1016/j.indcrop.2014.02.014>
43. Motaung TE, Linganisio LZ, Kumar R, Anandjiwada RD (2016) Agave and sisal fibre-reinforced polyfurfural alcohol composites. *J Thermoplast Compos Mater*. 30(10):1323–1343. <https://doi.org/10.1177/2F0892705716632858>
44. Mzimela ZNT, Linganisio LZ, Revaprasadu N, Motaung TE (2018) Comparison of cellulose extraction from sugarcane bagasse through alkali. *Mat Res* 21(6). <https://doi.org/10.1590/1980-5373-mr-2017-0750>
45. Nelson ML, O'Connor RT (1964) Relation of certain infrared bands to cellulose crystallinity and crystal latticed type. Part I. Spectra of lattice types I, II, III and of amorphous cellulose. *J Appl Polym Sci* 8:1321–1324. <https://doi.org/10.1002/app.1964.070080322>
46. Oh SY, Yoo DI, Shin Y, Seo G (2005) FTIR analysis of cellulose treated with sodium hydroxide and carbon dioxide. *Carbohydr Res* 340:417–428. <https://doi.org/10.1016/j.carres.2004.11.027>
47. Pathak P, Gupta A, Bhardwaj NK, Goyal A, Moholkar VS (2020) Impact of mild and harsh conditions of formic acid-based organosolv pretreatment on biomass fractionation of sugarcane tops. *Biomass Conv Bioref* 1–14. <https://doi.org/10.1007/s13399-020-00629-w>
48. Pereira PHF, Oliveira TÍS, Rosa MF, Cavalcante FL, Moates GK, Wellner N, Waldron KW, Azeredo HMC (2016) Pectin extraction from pomegranate peels with citric acid. *Int J Biol Macromol* 88:373–379. <https://doi.org/10.1016/j.ijbiomac.2016.03.074>
49. Pereira PHF, Ornaghi Júnior HL, Coutinho LV, Duchemin B, Cioffi MOH (2020) Obtaining cellulose nanocrystals from pineapple crown fibers by free-chlorite hydrolysis with sulfuric acid: physical, chemical and structural characterization. *Cellulose* 27:5745–5756. <https://doi.org/10.1007/s10570-020-03179-6>
50. Phanthong P, Reubroycharoen P, Hao X, Xu G, Abudula A, Guan G (2018) Nanocellulose: extraction and application. *Carbon Resour Conver* 1:32–43. <https://doi.org/10.1016/j.crcon.2018.05.004>
51. Pickering KL, Beckermann GW, Alam SN, Foreman NJ (2007) Optimising industrial hemp fibre for composites. *Compos Appl Sci Manuf* 38:461–468. <https://doi.org/10.1016/j.compositesa.2006.02.020>
52. Rajinipriya M, Nagalakshmaiah M, Robert M, Elkoun S (2018) Importance of agricultural and industrial waste in the field of nanocellulose and recent industrial developments of wood based nanocellulose: a review. *ACS Sustain Chem Eng* 6:2807–2828. <https://doi.org/10.1021/acssuschemeng.7b03437>
53. Ray D, Sarkar BK, Basak RK, Rana AK (2002) Study of the thermal behavior of alkali-treated jute fibers. *J Appl Polym Sci* 85:2594–2599. <https://doi.org/10.1002/app.10934>
54. Rezende CA, de Lima MA, Maziero P, deAzevedo E, Garcia W, Polikarpov I (2011) Chemical and morphological characterization of sugarcane bagasse submitted to a delignification process for enhanced enzymatic digestibility. *Biotechnol Biofuels* 4:54. <https://doi.org/10.1186/1754-6834-4-54>
55. Ruland W (1961) X-ray determination of crystallinity and diffuse disorder scattering. *Acta Cryst* 14:1180–1185. <https://doi.org/10.1107/S0365110X61003429>
56. Samal RK, Panda BB, Rout SK, Mohanty M (1995) Effect of chemical modification on FTIR spectra. I. Physical and chemical behavior of coir. *Appl Polym Sci* 58:745–752. <https://doi.org/10.1002/app.1995.070580407>
57. Segal LC, Creely J Jr, Martin AEJ, Conard CM (1959) An empirical method for estimating the degree of crystallinity of native cellulose using the x-ray diffractometer. *Text Res J* 29:786–794. <https://doi.org/10.1177/004051755902901003>
58. Singh M, Kaushik A, Ahuja D (2016) Surface functionalization of nanofibrillated cellulose extracted from wheat straw: effect of process parameters. *Carbohydr Polym* 150:48–56. <https://doi.org/10.1016/j.carbpol.2016.04.109>
59. Siró I, Plackett D (2016) Microfibrillated cellulose and new nanocomposite materials: a review. *Cellulose* 17:459–494. <https://doi.org/10.1007/s10570-010-9405-y>
60. Song Y, Jiang W, Zhang Y, Wang H, Zou F, Yu K, Han G (2018) A novel process of nanocellulose extraction from knaf bast. *Mater Res Express* 5(8)
61. Sun Y, Cheng J (2002) Hydrolysis of lignocellulosic materials for ethanol production: a review. *Bioresour Technol* 83:1–11. [https://doi.org/10.1016/S0960-8524\(01\)00212-7](https://doi.org/10.1016/S0960-8524(01)00212-7)
62. Sun D, Onyianta AJ, O'Rourke D, Perrin G, Popescu CM, Saw LH, Cai Z, Dorris M (2020) A process for deriving high quality cellulose nanofibrils from water hyacinth invasive species. *Cellulose* 27:3727–3740. <https://doi.org/10.1007/s10570-020-03038-4>
63. Tibolla H, Pelissari FM, Rodrigues MI, Menegalli FC (2017) Cellulose nanofibers produced from banana peel by enzymatic treatment: study of process conditions. *Ind Crop Prod* 95:674–674. <https://doi.org/10.1016/j.indcrop.2016.11.035>

64. Tu WC, Weigand L, Hummel M, Sixta H, Brandt-Talbot A, Hallett JP (2020) Characterisation of cellulose pulps isolated from *Miscanthus* using a low-cost acidic ionic liquid. *Cellulose* 27: 4745–4761. <https://doi.org/10.1007/s10570-020-03073-1>
65. Vanessa LA, Graziella AJ, Claudio APL, Luciano PS (2015) Cellulose nanocrystals obtained from rice by-products and their binding potential to metallic ions. *J Nanomate* 2015:article id: 357384. <https://doi.org/10.1155/2015/357384>
66. Viera RGP, Filho GR, de Assuncao RMN, Meireles CS, Vieira JG, de Oliveira GS (2007) Synthesis and characterization of methylcellulose from sugar cane bagasse cellulose. *Carbohydr Polym* 67: 182–189. <https://doi.org/10.1016/j.carbpol.2006.05.007>
67. Xie Y, Guo X, Ma Z, Gong J, Wang H, Lv Y (2020) Efficient extraction and structural characterization of hemicellulose from sugarcane bagasse pith. *Polymers* 12:608. <https://doi.org/10.3390/polym12030608>
68. Xu E, Wang D, Lin L (2020) Chemical structure and mechanical properties of wood cell walls treated with acid and alkali solution. *Forests* 11:87. <https://doi.org/10.3390/f11010087>
69. Zhang F-D, Xu C-H, Li M-Y, Huang A-M, Sun S-Q (2014) Rapid identification of *Pterocarpus santalinus* and *Dalbergia louvelii* by FTIR and 2D correlation IR spectroscopy. *J Mol Struct* 1069:89–95. <https://doi.org/10.1016/j.molstruc.2014.01085>
70. Zhou YM, Fu SY, Zheng LM, Zhan HY (2012) Effect of nanocellulose isolation technique on the formation of reinforced poly(vinyl alcohol) nanocomposite films. *Express Polm Lett* 6: 794–804. <https://doi.org/10.3144/expresspolymlett.2012.85>

Publisher's note Springer Nature remains neutral with regard to jurisdictional claims in published maps and institutional affiliations.